Volume 13
Number 29
7 August 2022
Pages 8447–8706

# Chemical Science

rsc.li/chemical-science


ISSN 2041-6539

ROYAL SOCIETY OF CHEMISTRY

**EDGE ARTICLE**

Chengzhong Yu *et al.*

Mesoporous sodium four-coordinate aluminosilicate nanoparticles modulate dendritic cell pyroptosis and activate innate and adaptive immunity

Chemical Science

ROYAL SOCIETY OF CHEMISTRY

EDGE ARTICLE

View Article Online
View Journal | View Issue



Cite this: *Chem. Sci.*, 2022, **13**, 8507

All publication charges for this article have been paid for by the Royal Society of Chemistry

# Mesoporous sodium four-coordinate aluminosilicate nanoparticles modulate dendritic cell pyroptosis and activate innate and adaptive immunity†

Jie Tang,‡[a] Yang Yang,‡[a] Jingjing Qu,[a] Wenhuang Ban,[a] Hao Song,[a] Zhengying Gu,[b] Yannan Yang,[a] Larry Cai,[a] Shevanuja Theivendran,[a] Yue Wang,[a] Min Zhang[b] and Chengzhong Yu *[ab]

Pyroptosis is a programmed cell death widely studied in cancer cells for tumour inhibition, but rarely in dendritic cell (DC) activation for vaccine development. Here, we report the synthesis of sodium stabilized mesoporous aluminosilicate nanoparticles as DC pyroptosis modulators and antigen carriers. By surface modification of sodium-stabilized four-coordinate aluminium species on dendritic mesoporous silica nanoparticles, the resultant Na-$^{IV}$Al-DMSN significantly activated DC through caspase-1 dependent pyroptosis *via* pH responsive intracellular ion exchange. The released proinflammatory cellular contents further mediated DC hyperactivation with prolonged cytokine release. *In vivo* studies showed that Na-$^{IV}$Al-DMSN induced enhanced cellular immunity mediated by natural killer (NK) cells, cytotoxic T cells, and memory T cells as well as humoral immune response. Our results provide a new principle for the design of next-generation nanoadjuvants for vaccine applications.

Received 25th September 2021
Accepted 20th June 2022

DOI: 10.1039/d1sc05319a

rsc.li/chemical-science



## Introduction

Pyroptosis is a programmed cell death triggered by caspase-1 after its activation by various pathological stimuli.[1] Recent studies have mainly focused on pyroptosis in tumor cells for cancer therapy,[2–7] such as using chemodrugs and metal-doped nanoparticles to generate reactive oxygen species (ROS).[8–10] During pyroptosis, danger-associated molecular patterns and proinflammatory cytokines such as interleukin-1 beta (IL-1β) and interleukin-18 (IL-18) are released, provoking a potent inflammatory response.[11–15] A similar process is also reported in lytic dendritic cells (DCs), resulting in hyperactive DCs with prolonged IL-1β secretion and enhanced T-cell responses.[16–18] As one important group of antigen-presenting cells,[19] DCs act as the body's first line of defence against invading pathogens. Upon pathogen infection, DCs undergo pyroptosis, which further recruits other immune cells like natural killer (NK) cells to directly fight against infectious pathogens or induce adaptive immune responses. The pyroptosis process comes with the cost of sacrificing a portion of DCs, but also with the benefits of activation of bystander DCs as compensation. Activated DCs secrete cytokines and present antigens to prime T cell responses against tumor or invading pathogens, thus bridging innate and adaptive immunity.[20–22] Various strategies such as nano-adjuvants,[23,24] agonists,[25] monoclonal antibodies,[26] and cytokines[27] have been used to activate DCs.[28–30] However, to the best of our knowledge, there are few reports using DC pyroptosis to stimulate the immune system in the design of cancer vaccines.

Sodium stabilized aluminosilicates with tetrahedral aluminum species (*e.g.* NaY and Na-ZSM-5) are a family of solid base catalysts with wide application in petrochemical cracking, water treatment, and removal of acidic gas molecules,[31–34] but are rarely used as vaccine adjuvants. Very recently, we reported mesoporous aluminosilicate nanoparticles modified with six-coordinate $^{VI}$Al–OH species (H-$^{VI}$Al-DMSNs) as adjuvants with endosomal escape performance and cellular immunity.[35] This design, however, is not capable of intracellular ion perturbation (*e.g.* $Na^+$ and $K^+$), which is a major cellular stress signal for the activation of inflammasome signalling that results in caspase-1 mediated pyroptosis.[36] A recent study showed that NaCl nanoparticles cause intracellular osmotic stress and Na/K imbalance, activating caspase-1-dependent pyroptosis in cancer cells.[6] It is also noted that conventional sodium stabilized aluminosilicates with micropores (pore size < 2 nm) can hardly be used as antigen carriers, and large mesopores are essential. Thus, the potential of the above materials in DC modulation and as antigen carriers in vaccine applications has not been reported.[31–36]

[a]*Australian Institute for Bioengineering and Nanotechnology, The University of Queensland, St Lucia, Brisbane, QLD 4072, Australia. E-mail: c.yu@uq.edu.au*

[b]*School of Chemistry and Molecular Engineering, East China Normal University, Shanghai 200241, China. E-mail: czyu@chem.ecnu.edu.cn*

† Electronic supplementary information (ESI) available. See https://doi.org/10.1039/d1sc05319a

‡ These authors contributed equally to this work.

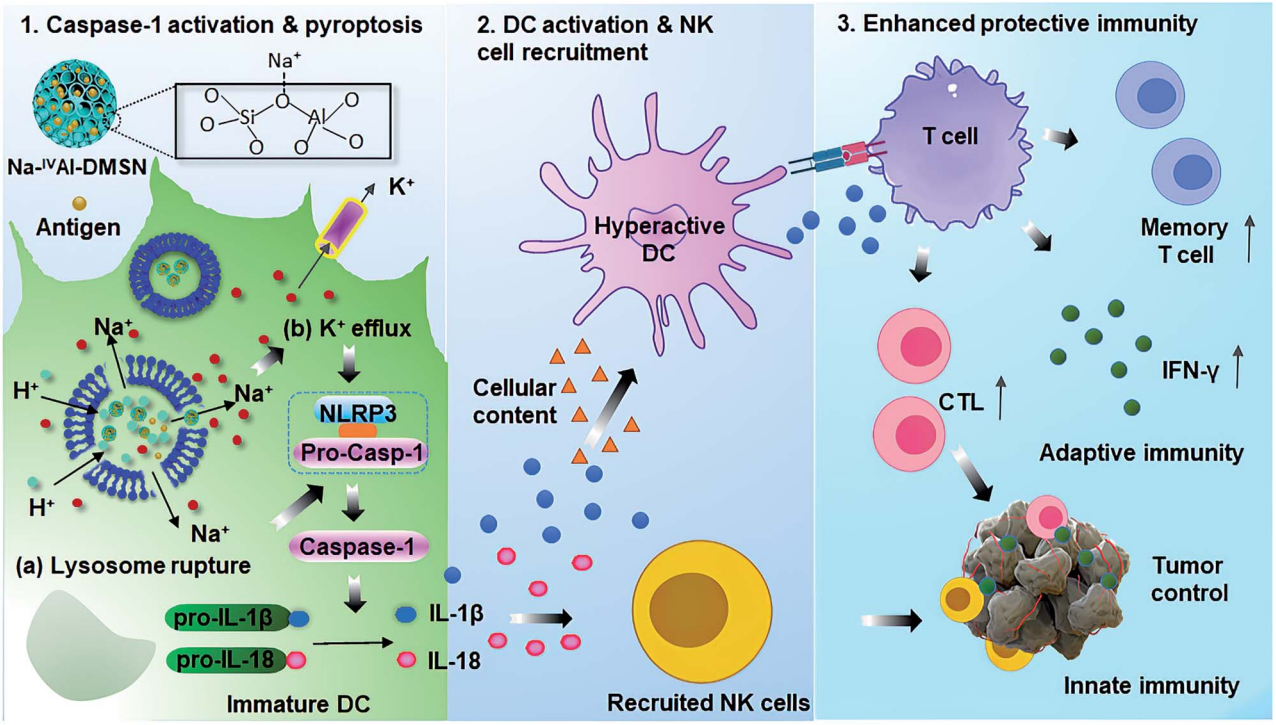


Scheme 1 Proposed mechanisms for Na-$^{IV}$Al-DMSN induced DC pyropotosis and hyperactivation for enhanced innate immunity and adaptive immunity for tumor prophylaxis.

In this work, we report the synthesis of sodium-stabilized dendritic mesoporous aluminosilicate nanoparticles with four-coordinate aluminium species (Na-$^{IV}$Al-DMSN) as nano-adjuvants for DC pyroptosis and hyperactivation. The designed Na-$^{IV}$Al-DMSN provides not only large mesopores (~30 nm) for antigen loading, but also basic sites as proton "sponges" for $H^+$ exchange and $Na^+$ sources in a pH-responsive manner (Scheme 1). After internalization of Na-$^{IV}$Al-DMSN by DCs, $H^+/Na^+$ exchange occurs in acidic lysosomes, leading to lysosome rupture, intracellular $Na^+$ increase/$K^+$ efflux, and caspase-1 dependent pyroptosis. The released cytokines including IL-1β, IL-18, and cellular contents from pyroptotic DCs mediate the hyperactivation of bystander DCs, which recruit NK cells and T cells, enhancing both adaptive cellular immunity and innate immunity for cancer treatment. The design of Na-$^{IV}$Al-DMSN, the use of mesoporous aluminosilicates as DC modulators and the underlying activation mechanism are rarely reported, providing new understandings and material design principles for vaccine applications.

## Results and discussion

Pure dendritic mesoporous silica nanospheres (DMSNs) were synthesized using an anion-assisted approach[37,38] (Fig. S1†), and then used as substrates to prepare Na-$^{IV}$Al-DMSN in an aqueous sodium aluminate solution (see the Experimental section). Transmission electron microscopy (TEM) images indicate that Na-$^{IV}$Al-DMSN has a uniform particle size of ~240 nm and typical centre-radial mesoporous channels (Fig. 1A and B), similar to bare DMSNs. The scanning electron microscopy (SEM) image in Fig. 1C shows open mesopores with large pore sizes of tens of nanometres and a wall thickness of ~8 nm, suggesting that the mesopores of DMSNs were not blocked during the post-modification process. The energy-dispersive X-ray spectroscopy (EDS) elemental mapping images (Fig. 1D) indicate that the Si, O, Na, and Al elements are uniformly distributed in Na-$^{IV}$Al-DMSN.

To demonstrate the unique structure and function of Na-$^{IV}$Al-DMSN, H-$^{IV}$Al-DMSN,[35] and Alhydrogel (a commercial adjuvant) were used as controls. H-$^{IV}$Al-DMSN exhibits a similar dendritic morphology to Na-$^{IV}$Al-DMSN (Fig. S2A–C†), except that there is no sodium in the silica framework (Fig. S2D–G†). The composition was quantified by inductively coupled plasma-optical emission spectroscopy (ICP-OES), showing 3.1% Al and 3.0% Na in Na-$^{IV}$Al-DMSN (Si/Al/Na ratio is 13.9/1/1.03) and 2.9% Al in H-$^{IV}$Al-DMSN (Si/Al ratio is 14.9/1). DMSNs, Na-$^{IV}$Al-DMSN, and H-$^{IV}$Al-DMSN exhibit similar particle sizes of ~220 nm (Fig. S3 and Table S1†). Moreover, Na-$^{IV}$Al-DMSN and H-$^{IV}$Al-DMSN are well-dispersed in various media (Table S1†), unlike Alhydrogel.[39,40] Na-$^{IV}$Al-DMSN and H-$^{IV}$Al-DMSN show comparable specific areas (360–380 $m^2\ g^{-1}$), pore volume (1.58–1.60 $cm^3\ g^{-1}$), and pore sizes (~30 nm).

Na-$^{IV}$Al-DMSN shows an amorphous nature as evidenced by the X-ray diffraction (XRD) pattern (Fig. 1E), similar to H-$^{IV}$Al-DMSN and DMSNs (Fig. S4†). Compared to pure $NaAlO_2$ and the physical mixture of DMSN + $NaAlO_2$, no characteristic peaks of $NaAlO_2$ were found in the XRD pattern of Na-$^{IV}$Al-DMSN, suggesting that $NaAlO_2$ reacted with silica during the post-

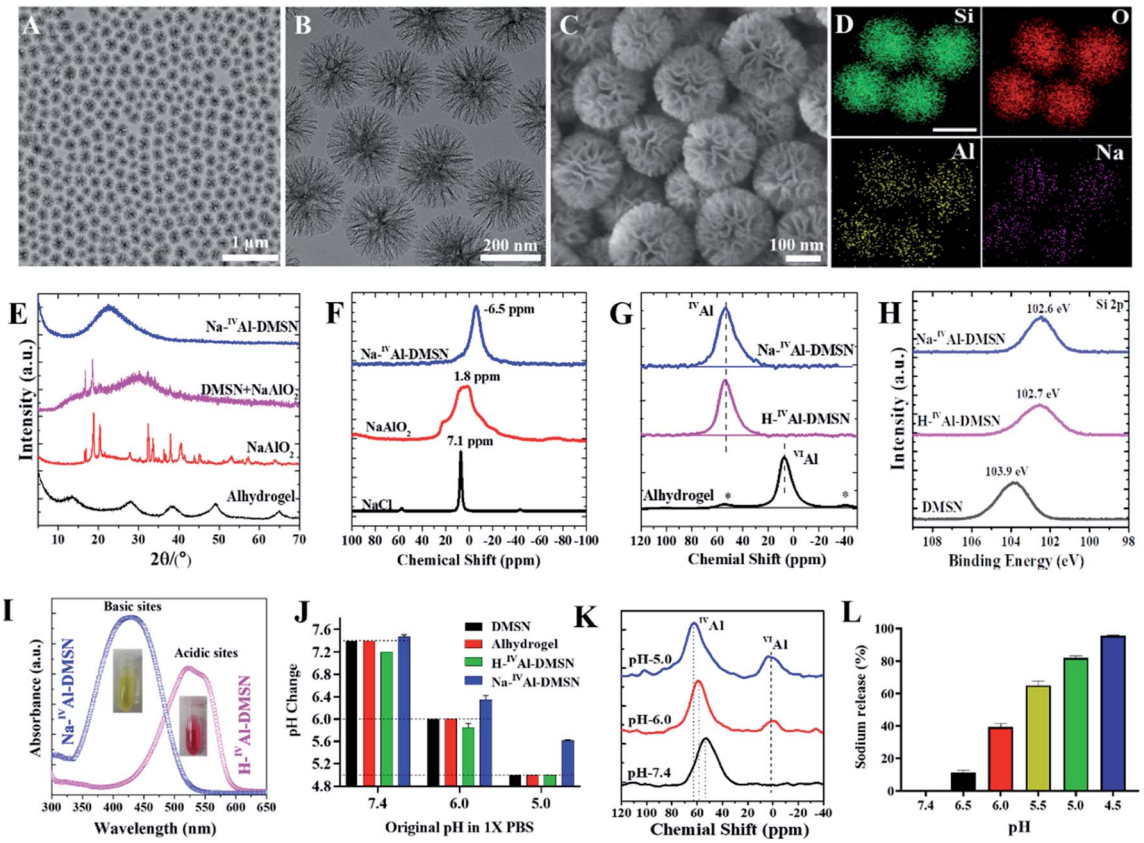


Fig. 1 Characterization of Na-$^{IV}$Al-DMSN. (A and B) TEM, (C) SEM and (D) EDS mapping (O, Si, Al and Na) images of Na-$^{IV}$Al-DMSN. (E) XRD patterns of Na-$^{IV}$Al-DMSN, DMSN + $NaAlO_2$, $NaAlO_2$, and Alhydrogel. (F) $^{23}$Na MAS NMR results of Na-$^{IV}$Al-DMSN, $NaAlO_2$, and NaCl. (G) 27Al MAS NMR results of Na-$^{IV}$Al-DMSN, H-$^{IV}$Al-DMSN, and Alhydrogel. (H) High-resolution XPS analysis (Si2p) of Na-$^{IV}$Al-DMSN in comparison with H-$^{IV}$Al-DMSN and DMSNs. (I) UV-vis absorption spectra of the methyl red solution incubated with Na-$^{IV}$Al-DMSN and H-$^{IV}$Al-DMSN (inset: digital photos). (J) The pH change of PBS with an initial pH of 7.4, 6.0, and 5.0 treated with Na-$^{IV}$Al-DMSN, H-$^{IV}$Al-DMSN, DMSN, and Alhydrogel. (K) The $^{27}$Al MAS NMR results of Na-$^{IV}$Al-DMSN after being treated with PBS with a pH of 7.4, 6.0 and 5.0. (L) The sodium release percentage of Na-$^{IV}$Al-DMSN in PBS with a pH of 7.4, 6.0, and 5.0.

modification process. The chemical structure was characterized by magic-angle spinning (MAS) nuclear magnetic resonance (NMR). As shown in $^{23}$Na MAS NMR (Fig. 1F), the chemical shift (−6.5 ppm) of Na-$^{IV}$Al-DMSN is similar to that of zeolite NaX/NaY, indicating that $Na^+$ in Na-$^{IV}$Al-DMSN interacts with the negatively charged O atom connected to Si and $^{IV}$Al (Si–O–$^{IV}$Al, see Scheme 1),[41–43] unlike $NaAlO_2$ and NaCl. $^{27}$Al MAS NMR studies (Fig. 1G) indicate the presence of only tetrahedral aluminum in Na-$^{IV}$Al-DMSN, evidenced by the chemical shift of Al from 75 ppm ($Al(OAl)_4$) in pure $NaAlO_2$ (Fig. S5†) to 53 ppm ($Al(OSi)_4$) in Na-$^{IV}$Al-DMSN. H-$^{IV}$Al-DMSN exhibits a similar chemical environment of Al to Na-$^{IV}$Al-DMSN, while Alhydrogel with a boehmite phase (evidenced by XRD, Fig. 1E) shows a typical octahedral structure of Al (centered at 7 ppm). The Si–O–Al bond formation in both H/Na-$^{IV}$Al-DMSN can be supported by the change in Si2p binding energy compared to DMSNs (Fig. 1H).

In classical crystalline aluminosilicates such as zeolite NaY, the sodium-stabilized Si–O–$^{IV}$Al species have been identified as the basic sites.[44] Qualitative measurement of the acid–base properties was performed by incubating samples in methyl red solution (Fig. 1I). Na-$^{IV}$Al-DMSN exhibits basicity as evidenced by the UV-vis absorbance peak centering at 435 nm (yellow color, inset of Fig. 1I). In contrast, H-$^{IV}$Al-DMSN exhibits acidity, reflected by the peak at 530 nm (red color). The basicity of Na-$^{IV}$Al-DMSN leads to $H^+/Na^+$ exchange behavior (Fig. S6†), more obviously at pH 5 than at pH 6 or 7.4 (Fig. 1J). Consequently, the formation of a portion of octahedral aluminum $^{VI}$Al species (chemical shift at 0–3 ppm) and the occurrence of $^{IV}$Al with higher chemical shifts (from 53 to 59 and 63 ppm when pH increased from 7.4 to 6.0 and 5.0) were observed in a pH dependent manner (Fig. 1K), indicating further hydrolysis and loss of silicate species from the proton-stabilized tetrahedral aluminum sites (Fig. S6†).[45] This mechanism is further supported by the increased $Na^+$ released percentage with decreased pH (Fig. 1L). The above results have demonstrated that Na-$^{IV}$Al-DMSN provides not only large mesopores, but also Lewis basic sites (Scheme 1) for proton exchange and as sodium sources in a pH-responsive manner (pH range of 7.4–5.0). Such a combination is rarely reported to the best of our knowledge.

With a unique structure, the potential of Na-$^{IV}$Al-DMSN as an antigen delivery vehicle and adjuvant was firstly studied. As shown in Fig. S7A,† when ovalbumin (OVA) was chosen as a model antigen, DMSNs, H-$^{IV}$Al-DMSN, and Na-$^{IV}$Al-DMSN

exhibited a similar loading capacity of 254–290 mg $g^{-1}$ without a significant difference, lower than that of Alhydrogel (446 mg $g^{-1}$). The OVA release profile was also determined. Less than 40% of the entrapped OVA was released from all the particles over 72 h (Fig. S7B†), showing a more sustained release profile compared to Alhydrogel. To monitor the antigen delivery performance of DMSNs, Na-$^{IV}$Al-DMSN, H-$^{IV}$Al-DMSN, and Alhydrogel into DC 2.4 cells, fluorescein isothiocyanate (FITC, a dye with green fluorescence) conjugated OVA (FITC-OVA) and flow cytometry were used. The results showed that all three DMSN-based formulations (Na-$^{IV}$Al-DMSN, H-$^{IV}$Al-DMSN, and DMSNs) significantly enhanced the uptake of FITC-OVA by DCs compared with FITC-OVA (Fig. S7C and D†). However, Alhydrogel showed higher mean fluorescence intensity of FITC-OVA compared to DMSN-based groups, presumably due to its high positive charge (Table S1†).

The cytotoxicity of DMSNs, H-$^{IV}$Al-DMSN, Na-$^{IV}$Al-DMSN and Anhydrogel was tested against a panel of cell lines by cellular metabolic activity assay. It was found that Na-$^{IV}$Al-DMSN showed high biocompatibility to Raw 264.7 (macrophages) and CT26 cancer cells up to 150 μg $mL^{-1}$, but a dose-dependent toxicity to DC2.4 cells from 20 μg $mL^{-1}$ (Fig. 2A). To understand this cell-type dependent cytotoxicity of Na-$^{IV}$Al-DMSN, the cellular uptake of Na-$^{IV}$Al-DMSN in DCs, Raw264.7, and CT26 cells was investigated. After incubation for 24 h, the intracellular Si contents determined by ICP-OES showed no significant difference in these cells (Fig. S8A†), suggesting that the selective cytotoxicity of Na-$^{IV}$Al-DMSN to DCs may not come from the selective internalization in DCs. Moreover, at the same dosage, Alhydrogel, DMSNs, and H-$^{IV}$Al-DMSN were less toxic to DCs compared to Na-$^{IV}$Al-DMSN (Fig. S8B†). The DC selective cytotoxicity of Na-$^{IV}$Al-DMSN is interesting, which is possibly associated with ion channels and intracellular ion perturbation.[46] Immature DCs highly express $Na_V1.7$, a voltage-gated sodium channel on the endosomal membrane, which is responsible for sensing pH changes and maintaining the membrane potential.[47,48] Thus, compared to other control samples, the internalized Na-$^{IV}$Al-DMSN with pH-dependent sodium release properties is more sensitive to DCs other than RAW 264.7 and CT26 cells.

To support our hypothesis, ICP-OES was conducted. A consistent increase of intracellular [$Na^+$] in DCs was observed when incubated with Na-$^{IV}$Al-DMSN for 12 h (Fig. 2B), significantly different from other groups. A decrease in intracellular [$K^+$] was also observed after 6 h incubation with Na-$^{IV}$Al-DMSN compared with other control groups (Fig. 2C), possibly as

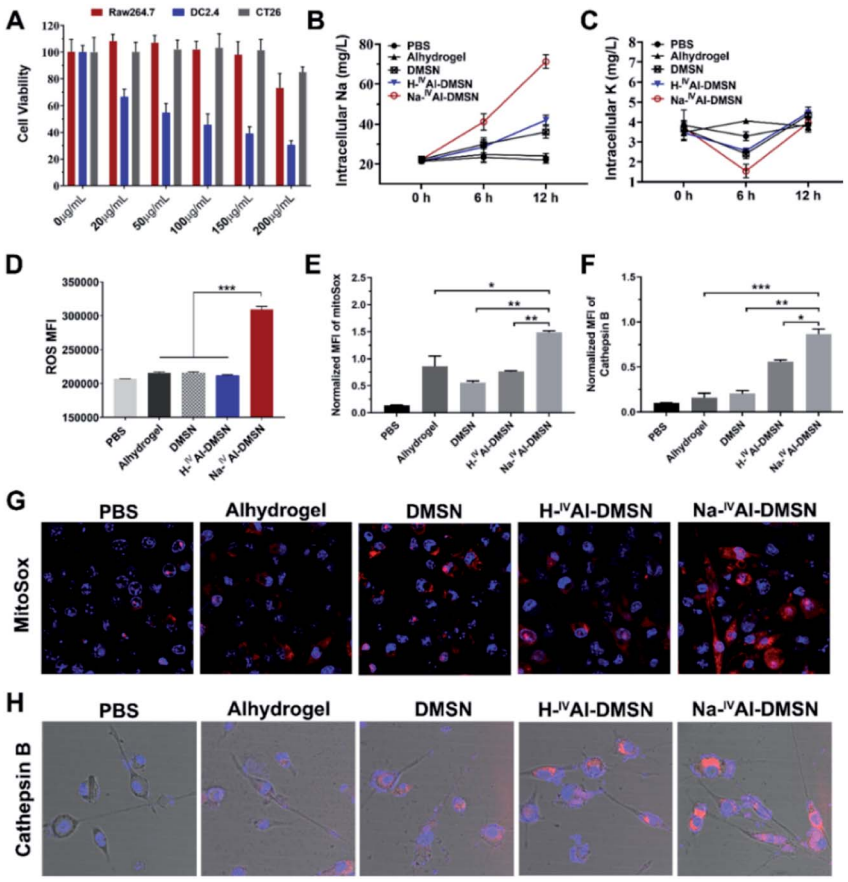


Fig. 2 Na-$^{IV}$Al-DMSN induced cytosolic perturbations. (A) Cell line-dependent cytotoxicity measured by MTT assays. Intracellular (B) sodium and (C) potassium concentration changes at different time points. Intracellular (D) ROS, (E) mitochondrial stress levels and (F) cathepsin B release after 6 h incubation of Alhydrogel, DMSN, H-$^{IV}$Al-DMSN, and Na-$^{IV}$Al-DMSN with DC2.4 cells. PBS treated cells were studied as controls. The CLSM images of (G) MitoSox (red, representing mitochondrial ROS) and (H) Magic Red (representing cathepsin B) stained DCs. Blue, DAPI (nucleus).

a result of $K^+$ efflux in response to the increased $[Na^+]$ and cytosol osmolarity. It was reported that for activated DCs, $Na_v1.7$ was downregulated whereas $K_v1.3$ (a $K^+$ channel) was upregulated.[48] The inward shift of $K^+$ from 6 to 12 h is possibly due to the $Na^+K^+$-ATPase pump and upregulated $K_v1.3$, which shuffle $Na^+$ extracellularly and transfer $K^+$ intracellularly to maintain osmotic equilibrium and membrane potential.[49]

Studies have shown that a decrease in intracellular $[K^+]$ is an essential trigger for inflammasome activation in immune cells such as DCs,[50] in addition to other stress induced by ROS, mitochondrion dysfunction, lysosome disruption, *etc.*[51–53] These signalling messengers in DCs were also measured. As shown in Fig. 2D, Na-$^{IV}$Al-DMSN generated the highest level of ROS among all the treated groups. Moreover, Na-$^{IV}$Al-DMSN promoted a ~2-fold increase in mitochondrial-specific stress (indicated by MitoSox fluorescence) compared to DMSN, H-$^{IV}$Al-DMSN, and Alhydrogel (Fig. 2E and G). This is because mitochondria are sensitive to cytosol osmolarity changes.[54] In addition, the release of lysosomal cathepsin B is an indicator of lysosome disruption.[55] Na-$^{IV}$Al-DMSN induced the highest cathepsin B level as shown in Fig. 2H (quantified results in Fig. 2F), indicating that Na-$^{IV}$Al-DMSN with $H^+/Na^+$ exchange properties can induce lysosome rupture.

Previous studies showed that decreases in intracellular $[K^+]$, mitochondrial dysfunction, and cytosolic release of cathepsin-B induced inflammasome and caspase-1 activation.[53,56] Hence, it is reasonable to infer that Na-$^{IV}$Al-DMSN could also activate DCs and possibly caspase-1 mediated pyroptosis.[57] We validated this hypothesis by measuring cleaved caspase 1, IL-1β, and IL-18 release from DCs. As shown in Fig. 3A, Na-$^{IV}$Al-DMSN treatment led to significantly increased caspase-1 activity (FAM-FLICA staining, a caspase-1-specific marker) compared to the control. The inefficiency of Alhydrogel in caspase-1 activation in DCs in the absence of toll-like receptor (TLR) agonists is consistent with a literature report.[58]

Pyroptosis is dependent on caspase-1 activation and causes pore formation on the cell membrane.[15] To investigate whether Gasdermin-D (GSDMD), a recently identified mediator of pyroptosis, mediates the pore formation directly, we examined the expression of the cleaved GSDMD in DC2.4 cells after being incubated with different formulations by the western blot. As shown in Fig. 3B, cleaved GSDMD expression was significantly higher in Na-$^{IV}$Al-DMSN treated DCs compared to PBS, H-$^{IV}$Al-DMSN or Alhydrogel groups. This observation is in accordance with the higher activation of caspase-1 in Na-$^{IV}$Al-DMSN treated DCs (Fig. 3A), as GSDMD was cleaved by caspase-1 in inflammasomes, and the proteolytic cleavage of GSDMD mediates pyroptosis and IL-1β secretion.[59] The cleaved GSDMD expression in Na-$^{IV}$Al-DMSN treated DCs was even higher than that after LPS + nigericin treatment (positive control). Interestingly, we found that there is no significant difference in cleaved GSDMD levels in Na-$^{IV}$Al-DMSN treated DCs with or without LPS-priming, indicating that Na-$^{IV}$Al-DMSN can initiate pyroptosis through the formation of pores on the plasma membrane even without LPS-priming.

To further test pyroptosis in DCs, propidium iodide (PI, a membrane-impermeant nucleic acid intercalator) and FAM-FLICA were co-employed to examine pyroptosis in DCs *via* flow cytometry. DCs treated with Na-$^{IV}$Al-DMSN showed a higher level of pyroptosis compared to other groups (Fig. 3C and S9†). The morphological features of DC2.4 cells incubated with Na-$^{IV}$Al-DMSN were also investigated using microscopy. Na-$^{IV}$Al-DMSN treated DCs showed a typical morphology change during pyroptosis similar to LPS + nigericin treated DCs, with pyroptotic body formation, cell flattening, and plasma membrane pore formation[11,60] (Fig. S10†). The activation of caspase-1 dependent pyroptosis caused elevated IL-1β (Fig. 3D) and IL-18 (Fig. 3E) secretion in the Na-$^{IV}$Al-DMSN group. The co-stimulatory surface marker (CD40, CD80, and CD86) expression and Th1-polarized cytokine (IFN-γ, TNF-α, and IL-12) secretion of DCs were also tested. In all cases the Na-$^{IV}$Al-DMSN group showed the highest level in all tested groups (Fig. S11†). Flow cytometry results also indicate that Na-$^{IV}$Al-DMSN efficiently delivered the OVA antigen to DCs and mediated potent cross-presentation by MHC class I molecules (Fig. 3F). The enhanced DC maturation, elevated secretion of Th1-polarized cytokines, and cross-presentation of the carried antigen indicate the potential of Na-$^{IV}$Al-DMSN as an efficient adjuvant to promote the cellular immunity.

It was reported that the release of IL-1β, IL-18, and cellular content from pyroptotic DCs further amplified the inflammatory response of bystander DCs, resulting in the second state of DC 'hyperactivation'. These hyperactive DCs are superb activators of T cells that enhance adaptive immunity.[16,61] Hyperactive DCs were also reported to produce IL-1β independent of pyroptosis for a longer period compared to classical activated DCs such as those treated with adjuvants.[16] The potential of Na-$^{IV}$Al-DMSN in inducing hyperactive DCs was tested (see the flow chart, Fig. 3G). Immature DCs incubated with the supernatants composed of cellular components released from pyroptotic DCs, followed by incubation in fresh medium, secreted a significantly higher amount of IL-1β in fresh medium within 24 h, nearly one order of magnitude higher than that from DCs first treated with Na-$^{IV}$Al-DMSNs and then incubated in fresh medium (Fig. 3H), suggesting DC hyperactivation. The morphology of DCs was investigated by staining the cells with rhodamine phalloidin. Confocal images show that immature DCs display a round morphology with a relatively smooth surface, while hyperactive DCs appear slightly elongated with numerous spines on the surface (Fig. 3I), corresponding to the morphology of hyperactive DC reported in the literature.[16]

It is known that a large population of DCs are located in the lymph nodes. To assess whether the OVA loaded Na-$^{IV}$Al-DMSN could efficiently migrate to lymph nodes, *in vivo* imaging of the depot and lymph node was conducted. Na-$^{IV}$Al-DMSN not only increased OVA-FITC accumulation in proximal lymph nodes but also promoted OVA-FITC transportation from the injection site to the distal lymph nodes (Fig. S12†). As lymph nodes are peripheral lymphoid organs where activated DCs can interact with T cells and B cells to initiate an adaptive immune response, Na-$^{IV}$Al-DMSN offers a better chance to induce an effective immune response.[62]

To investigate whether Na-$^{IV}$Al-DMSN is able to induce cellular immunity against tumours *in vivo*, the vaccine adjuvant

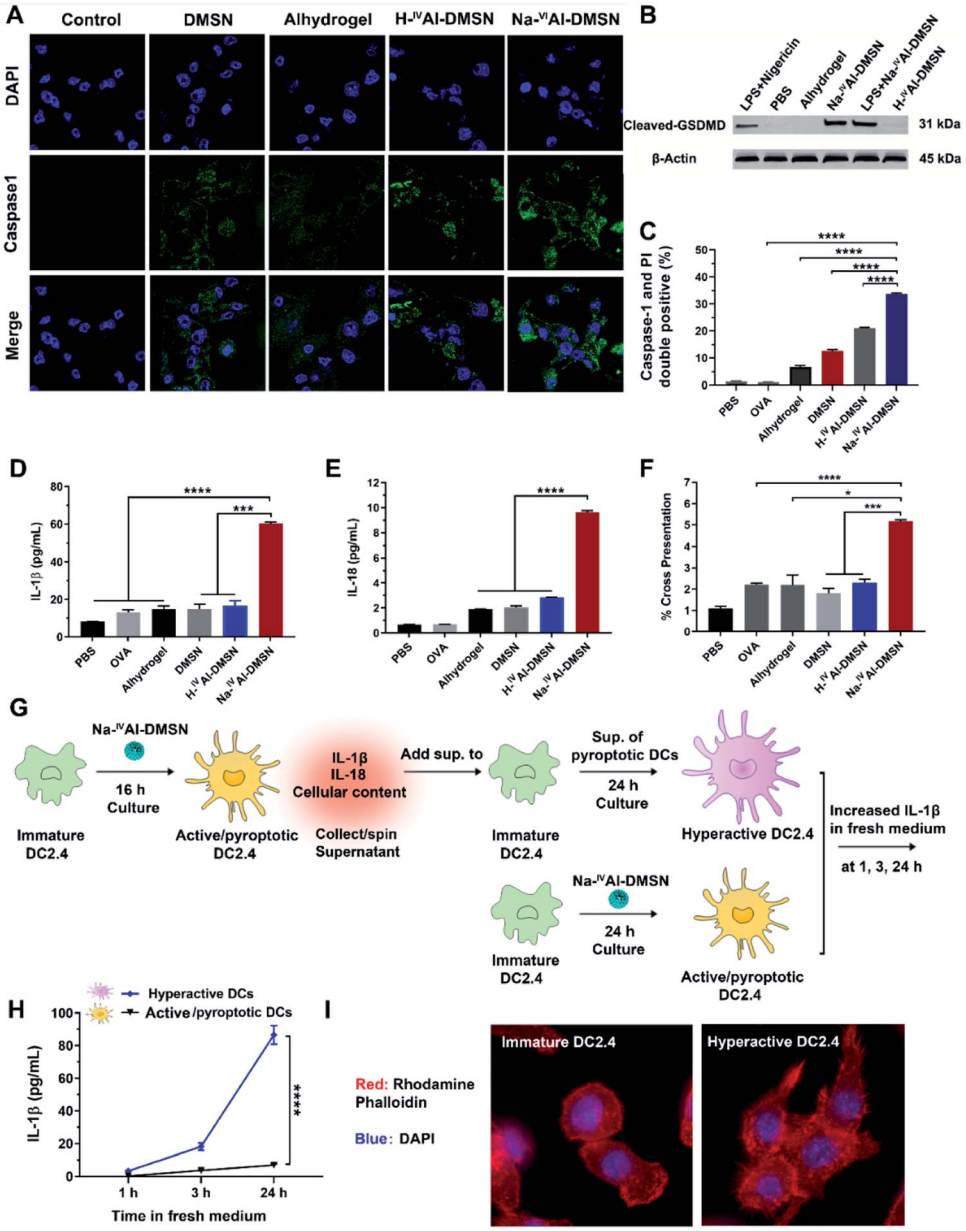


Fig. 3 Na-$^{IV}$Al-DMSN induced DC pyroptosis and DC pyroptosis-meditated DC hyperactivation. (A) Confocal microscopy to evaluate caspase-1 activation. DC2.4 cells were incubated with Alhydrogel, DMSNs, H-$^{IV}$Al-DMSN, and Na-$^{IV}$Al-DMSN for 6 h and stained with a FAM-FLICA caspase-1 Assay kit. PBS was used as a negative control. Blue, DAPI (nucleus); green, caspase-1. (B) Western blot analysis of the cleaved GSDMD expression. DC2.4 cells were treated with Na-$^{IV}$Al-DMSN for 3 h and 6 h. Cleaved GSDMD western blot of cell lysates from DC 2.4 incubated with PBS, H-$^{IV}$Al-DMSN, and Alhydrogel for 6 h, and LPS-primed DCs incubated with Na-$^{IV}$Al-DMSN (6 h) were studied as controls. Cells treated with lipopolysaccharides (LPSs) (50 ng mL$^{-1}$, 4 h), followed by nigericin (10 μM, 2 h)-induced pyroptotic DCs were used as positive controls; β-actin was the loading control. (C) PI and FAM-FLICA co-staining to examine DC pyroptosis *via* flow cytometry. (D) IL-1β and (E) IL-18 were analyzed using an ELISA kit in DC culture supernatants incubated with various formulations for 24 h. (F) Cross-presentation of DCs incubated with different formulations loaded with OVA for 24 h assessed by flow cytometry. (G) A flow chat for assessing hyperactive DCs. Immature DC2.4 cells were firstly cultured with Na-$^{IV}$Al-DMSN for 16 h to obtain mature/pyroptotic DC2.4 cells. The supernatants from mature/pyroptotic DC2.4 cells were collected after spinning to remove cell pellets and nanoparticles, and then added to immature DC2.4 cells and incubated for 24 h to induce DC hyperactivation. Active/pyroptotic DC2.4 cells obtained from incubation of immature DCs and Na-$^{IV}$Al-DMSN for 24 h were used as controls. (H) IL-1β released from hyperactive and Active/pyroptotic DCs after incubation in fresh medium for 1, 3, and 24 h. (I) Confocal images showing the morphological change of hyperactive DC2.4 cells.

potency of Na-$^{IV}$Al-DMSN was examined in a prophylactic colon tumor model, in which the mice were immunized with NPs loaded with CT26 cell lysates subcutaneously three times (Fig. 4A). Seven days after the third immunization, the mice were challenged with CT26 cells and tumor growth was monitored every other day. As presented in Fig. 4B, mice treated with PBS exhibited a rapid increase in tumor volumes. The DMSN, H-$^{IV}$Al-DMSN, and Alhydrogel groups showed only slight

inhibition of tumor growth. However, the injection of the Na-$^{IV}$Al-DMSN group significantly decreased the tumour growth (Fig. 4B and S11A†). Meanwhile, there was no significant body weight drop throughout the study (Fig. S11B†).

Mice were euthanized on day 16 post tumor challenge. Tumor, spleen, and blood were harvested for analysis. An immunohistochemistry approach was adopted to determine whether caspase-1 in lymphocytes in the spleen was activated (Fig. 4C, upper panel). Cleaved caspase-1 density within the spleen sections was significantly higher in the Na-$^{IV}$Al-DMSN group than in all control groups, suggesting the induction of caspase-1 activation in the spleen in *vivo* by Na-$^{IV}$Al-DMSN (Fig. 4D). Terminal deoxynucleotidyl transferase dUTP nick-end labeling (TUNEL) analyses were also conducted for the excised tumors (Fig. 4C, lower panel). TUNEL assays found extensive positive staining in Na-$^{IV}$Al-DMSN treated tumors, indicating that the Na-$^{IV}$Al-DMSN formulation induced potent tumor cell apoptosis for tumor suppression (Fig. 4E). In addition, compared to the PBS control group, no remarkable pathological abnormalities were observed in H&E staining of major organs, including the heart, kidneys, and spleen (Fig. S13†).

To understand Na-$^{IV}$Al-DMSN boosted immune responses, DC infiltration and activation were also monitored.[16,63] Compared to the control, an increased level of activated DCs ($CD80^+CD86^+$) was observed in the spleen in the Na-$^{IV}$Al-DMSN group (Fig. 4F). Moreover, stronger activation of memory T cells in spleens ($CD44^+CD62L^-CD8^+$) in the Na-$^{IV}$Al-DMSN immunized group was observed, which are more effective invaders than other types of T cells, but barely activated by Alhydrogel,[16] DMSNs, or H-$^{IV}$Al-DMSN (Fig. 4I). Furthermore, serum was harvested from vaccinated mice and the levels of IFN-γ and IL-18 were quantified by ELISA. As shown in Fig. 4G and H, Na-$^{IV}$Al-DMSN stimulated the highest amount of IL-1β and IL-18 production compared to other groups. The observation is in agreement with the increased NK population, as the release of IL-1β and IL-18 augments the activity of NK cells.[64]

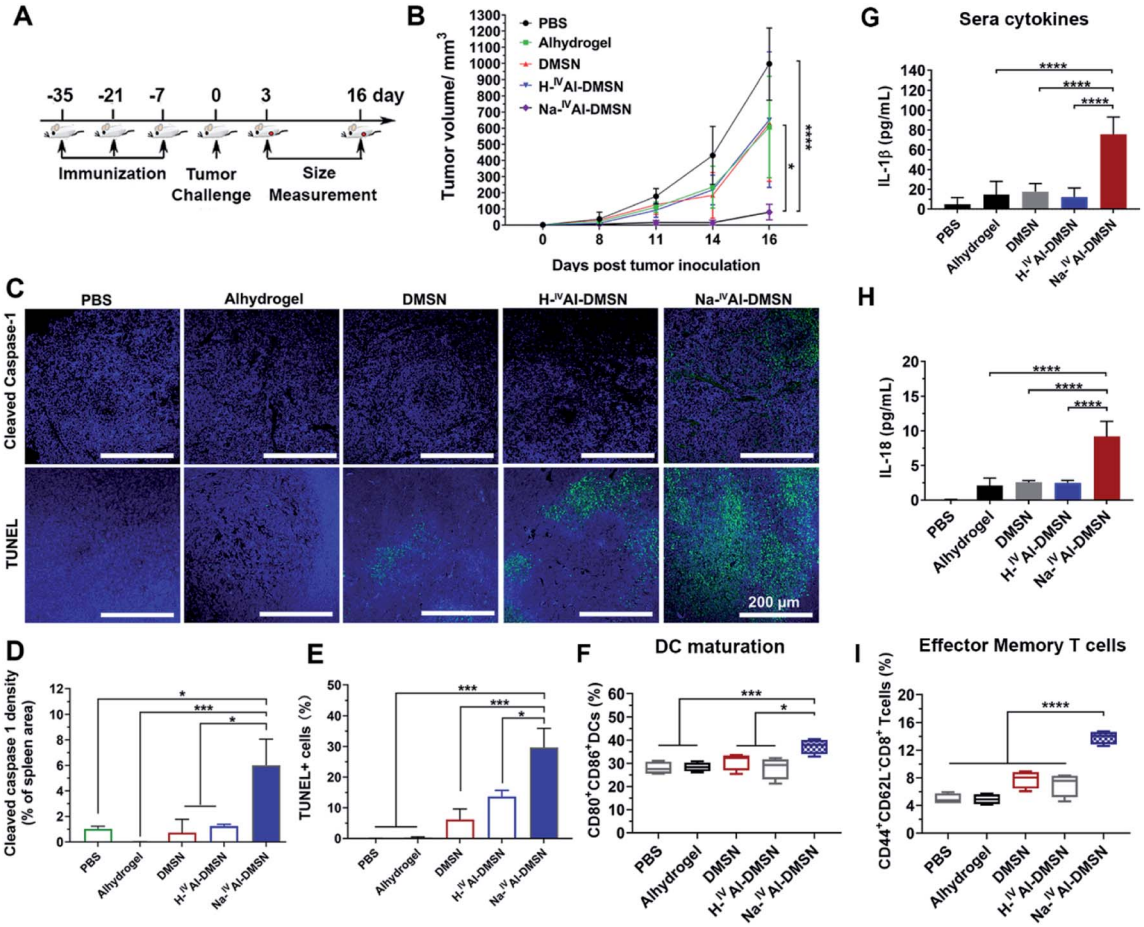


Fig. 4 Na-$^{IV}$Al-DMSN induced anti-cancer immunity in prophylactic tumor models using CT26 cell lysates as antigens. (A) Schematic illustration of the experimental protocol for the prophylactic tumor model. Balb/c mice were immunized subcutaneously with three doses of different vaccines as presented in Fig. 4A. (B) Tumor growth curves of mice after different immunizations. (C) Post-mortem histopathology on spleen tissues by cleaved caspase-1 staining and on tumor tissues by TUNEL staining. Quantification of (D) cleaved caspase-1 density in spleen sections and (E) TUNEL staining in tumor sections are expressed as mean ± SD from at least three independent experiments. Spleens were collected on day 16 for flow cytometry analysis. Flow cytometry analysis of splenocyte profiles of (F) $CD80^+CD86^+$DCs and (I) CD44highCD62LlowCD8$^+$T cells (effector memory T cells). Blood was collected for detecting the secretion of (G) IL-1β and (H) IL-18 using ELISA. Data are presented as mean ± SD (*$p$ < 0.05, **$p$ < 0.01, and ***$p$ < 0.005).

The cellular immune responses evoked by Na-$^{IV}$Al-DMSN were further investigated, which are essential for cancer vaccine performance. Na-$^{IV}$Al-DMSN formulation led to increased $CD8^+$ T cell and $CD4^+$ T cell population, significantly higher compared to all control groups in both splenocytes and tumor samples (Fig. S14A and B†). Moreover, mice immunized with Na-$^{IV}$Al-DMSN showed a significant increase in the percentages of $CD8^+$ and $CD4^+$ T cells that produced IFN-γ (so-called cytotoxic T lymphocyte, CTL) compared with all control groups (Fig. 5A and B), indicating an increase in the population of CTL that contributed to tumor prevention. NK cells play an important role in immune response.[65–67] Interestingly, the NK cell population (Fig. S14C†) as well as the IFN-γ released by NK cells (Fig. 5C) after being immunized by Na-$^{IV}$Al-DMSN were also elevated relative to other controls, suggesting that the cytolytic functions of NK cells towards tumor cells also contributed to the enhanced antitumor performance.

To further highlight the benefits of pyroptosis mediated cellular immunity induced by Na-$^{IV}$Al-DMSN (*e.g.*, endogenous cytokine production mediated by DC pyroptosis), its tumor inhibition efficiency and anti-cancer immunity were compared to three reported strategies in a prophylactic colon cancer model. The control groups include a commercial adjuvant Alhydrogel combined with 0.2 μg of exogenous IL-1β per mouse,[68] monophosphoryl lipid A (MPL, a TLR4 agonist used as a cancer vaccine adjuvant in clinic[69]), and H–$^{VI}$Al-DMSN with a six-coordinate environment but without $Na^+$ in the composition prepared using a different strategy.[35] The tumor growth curve and the digital images of tumors are shown in Fig. S15A and B,† respectively. Although combined with exogenous IL-1β, the Alhydrogel group had negligible tumor inhibition capability compared to the PBS control group. While MPL and H–$^{VI}$Al-DMSN moderately improved the tumor growth inhibition compared to the Alhydrogel + IL-1β group, Na-$^{IV}$Al-DMSN immunization decreased the tumor growth more significantly than all the other control groups.

Mice were euthanized on day 14 post tumor challenge. Tumor, spleen, and blood were harvested for analysis. Serum was harvested and the levels of IL-1β and IL-18 were quantified by ELISA. As shown in Fig. S15C and D,† Na-$^{IV}$Al-DMSN stimulated the highest cytokine levels among all groups under test, more significant in IL-18 production. The mice group immunized with H–$^{VI}$Al-DMSN exhibited significantly higher secretion levels of IL-1β compared to PBS, MPL, and Alhydrogel + IL-1β groups, but a similar secretion level of IL-18. The evoked cellular immune responses were further investigated. Mice immunized with Na-$^{IV}$Al-DMSN showed the strongest activation of NK cells, cytotoxic NK cells, $CD8^+$ T cells, and IFN-$\gamma^+CD8^+$ cells (Fig. S16A–D,† respectively) in tumor sites among all formulations. Moreover, stronger activation of memory T cells in spleens (Fig. S16E†) and DC maturation (Fig. S16F†) in the Na-$^{IV}$Al-DMSN immunized group was observed compared to control groups.

The above results indicate that endogenous cytokines produced by Na-$^{IV}$Al-DMSN are more efficient in evoking antitumor cellular immunity than Alhydrogel + exogenous IL-1β, consistent with a report showing that effective IL-1β secretion enhanced memory T cell activation.[16–18] MPL is a TLR4 agonist with potent adjuvant activity, *i.e.*, DC activation and effector memory CD8 T cell generation.[70] However, MPL alone does not

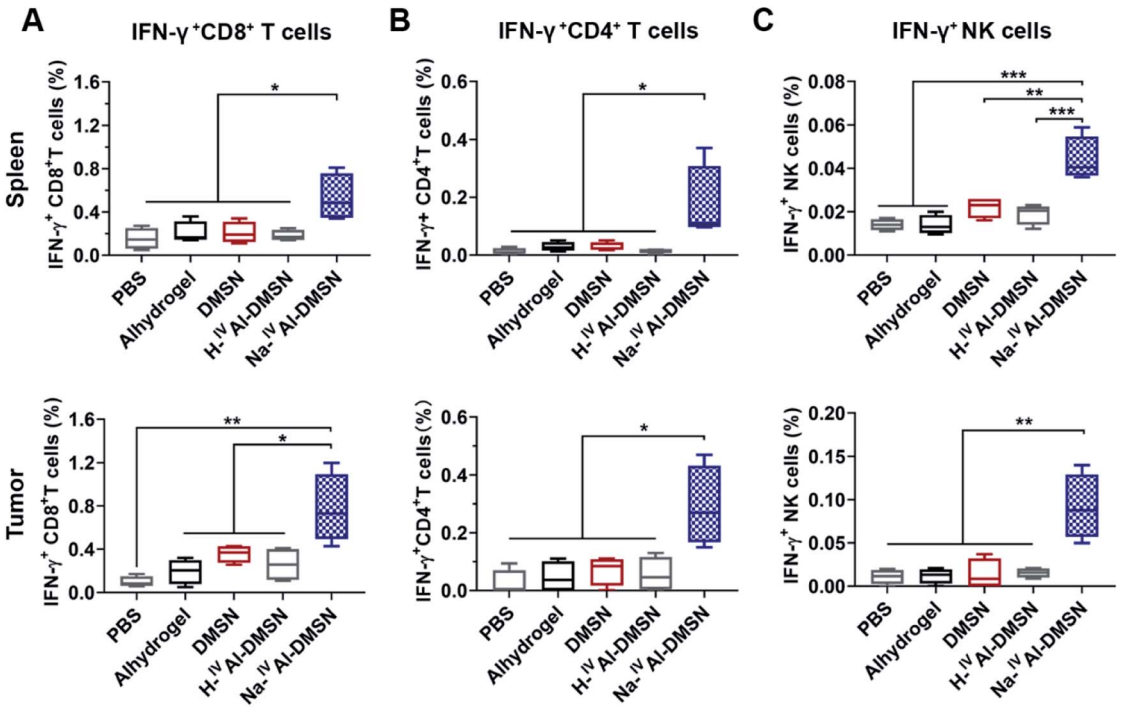


Fig. 5 Flow cytometry analysis of splenocyte profiles and tumor tissue samples collected on day 16 including: (A) $CD8^+$IFN-$\gamma^+$ T cells, (B) $CD4^+$IFN-$\gamma^+$ T cells, and (C) IFN-$\gamma^+$ NK cells. Data are presented as mean ± SD (*$p$ < 0.05, **$p$ < 0.01, and ***$p$ < 0.005).

induce proper cytotoxic T cell response,[71] in accordance with our observations (Fig. S16D and E†). Additionally, these observations are consistent with a previous report that H-$^{VI}$Al-DMSN with Brønsted basic $^{VI}$Al–OH sites enhanced the maturation of antigen presenting cells and provoke cellular immunity to some extent.[35] However, the H-$^{VI}$Al-DMSN design does not provide the capability of intracellular ion perturbation (*e.g.* $Na^+/K^+$ imbalance), which is a key cellular stress signal for the activation of inflammasome and caspase-1 mediated pyroptosis.[36] Therefore, Na-$^{IV}$Al-DMSN with pyroptosis triggering capability is more efficient in promoting anti-tumor cellular immune responses.

The therapeutic efficacy of this anti-tumor cellular response was confirmed in a mouse CT26 therapeutic model. Na-$^{IV}$Al-DMSN loaded with CT26 cell lysates delivered in two injections effectively delayed CT26 tumor growth (Fig. S18†). Compared with the other groups, mice immunized with Na-$^{IV}$Al-DMSN showed a significant increase in $CD8^+$ IFN-$\gamma^+$ T cells and IFN-$\gamma^+$ NK cells in tumor, and enhanced effector memory T cell activation and DC maturation in the spleen (Fig. S19†).

To demonstrate the potential of Na-$^{IV}$Al-DMSN as a nanoadjuvant in vaccination for diseases requiring antibody production in addition to cellular immunity, for example, virus infections, humoral immune response induced by Na-$^{IV}$Al-DMSN was evaluated using OVA as a model antigen. Three subcutaneous vaccinations fortnightly with OVA loaded Na-$^{IV}$Al-DMSN, H-$^{IV}$Al-DMSN, DMSN, and Alhydrogel were injected into C57BL/6 mice. Free OVA in PBS was used as a control. Fourteen days after the third immunization, blood was withdrawn for the analysis of OVA-specific antibody and cytokine production (Fig. S20A†). Na-$^{IV}$Al-DMSN showed the highest production of OVA-specific total IgG in blood among all the groups (Fig. S20B†). IgG1 and IgG2a are typical markers for Th2- and Th1-type immune responses, respectively. Na-$^{IV}$Al-DMSN enhanced the production of not only IgG1 (Fig. S20C†), but also IgG2a dramatically (Fig. S20D†). The Th1 polarized immunity of Na-$^{IV}$Al-DMSN is significantly enhanced compared to Alhydrogel, DMSN, and H-$^{IV}$Al-DMSN, which is further supported by the increased cytokine production including IL-1β and IFN-γ (Fig. S20E and F†). It is concluded that Na-$^{IV}$Al-DMSN can be used as a nanoadjuvant that induces potent cellular and humoral immunity in protection against viral challenges.

## Conclusions

In summary, novel Na-$^{IV}$Al-DMSN has been fabricated as a DC modulator and advanced adjuvant in vaccine formulations. Due to the unique pH-responsive $H^+/Na^+$ exchange properties, Na-$^{IV}$Al-DMSN particles induce intracellular ion perturbation and DC pyroptosis and hyperactivation,[16] provoking enhanced NK cell mediated innate immunity, and both cellular and humoral immune responses. The current study sheds light on the rational design of advanced adjuvants and DC modulators for vaccine applications.

## Data availability

All experimental supporting data are provided in the ESI.†

## Author contributions

C. Y., J. T. and Y. Y. initiated the idea, designed the experiments and wrote the manuscript. J. T. and Y. Y. synthesized the materials and conducted all of the *in vitro* experiments. J. T., J. Q., Z. G. and Y. Y. carried out the animal studies; W. B. helped with material synthesis and *in vitro* experiments. H. S., L. C., W. B., Y. W., S. T., and M. Z. assisted with the materials characterization. All authors contributed to the manuscript.

## Conflicts of interest

There are no conflicts to declare.

## Acknowledgements

The authors acknowledge the support from the Australian Research Council, the Australian National Fabrication Facility and the Australian Microscopy and Microanalysis Research Facility at the Centre for Microscopy and Microanalysis, The University of Queensland. This work was performed in part at the Queensland node of the Australian National Fabrication Facility, a company established under the National Collaborative Research Infrastructure Strategy to provide nano- and micro-fabrication facilities for Australia's researchers. All animal work was performed in accordance with Animal Ethics (AIBN/489/16) approved by the University of Queensland Institutional Animal Care and Use Committee.

## Notes and references

1 E. A. Miao, I. A. Leaf, P. M. Treuting, D. P. Mao, M. Dors, A. Sarkar, S. E. Warren, M. D. Wewers and A. Aderem, *Nat. Immunol.*, 2010, **11**, 1136–1142.
2 A. Dasgupta, M. Nomura, R. Shuck and J. Yustein, *Int. J. Mol. Sci.*, 2017, **18**, 23.
3 X. Huang, F. Xiao, Y. Li, W. Qian, W. Ding and X. Ye, *J. Exp. Clin. Cancer Res.*, 2018, **37**, 310.
4 J.-X. Fan, R.-H. Deng, H. Wang, X.-H. Liu, X.-N. Wang, R. Qin, X. Jin, T.-R. Lei, D. Zheng and P.-H. Zhou, *Nano Lett.*, 2019, **19**, 8049–8058.
5 P. Zhao, M. Wang, M. Chen, Z. Chen, X. Peng, F. Zhou, J. Song and J. Qu, *Biomaterials*, 2020, 120142.
6 W. Jiang, L. Yin, H. Chen, A. V. Paschall, L. Zhang, W. Fu, W. Zhang, T. Todd, K. S. Yu and S. Zhou, *Adv. Mater.*, 2019, **31**, 1904058.
7 D. Wu, S. Wang, G. Yu and X. Chen, *Angew. Chem., Int. Ed.*, 2021, **133**(15), 8096–8112.
8 X. Xia, X. Wang, Z. Cheng, W. Qin, L. Lei, J. Jiang and J. Hu, *Cell Death Dis.*, 2019, **10**, 1–13.
9 C. Xu, Y. Yu, Y. Sun, L. Kong, C. Yang, M. Hu, T. Yang, J. Zhang, Q. Hu and Z. Zhang, *Adv. Funct. Mater.*, 2019, **29**, 1905213.
10 Z. Wang, Y. Zhang, E. Ju, Z. Liu, F. Cao, Z. Chen, J. Ren and X. Qu, *Nat. Commun.*, 2018, **9**, 1–14.
11 Y. Zhang, X. Chen, C. Gueydan and J. Han, *Cell Res.*, 2018, **28**, 9–21.

12 J. Shi, Y. Zhao, K. Wang, X. Shi, Y. Wang, H. Huang, Y. Zhuang, T. Cai, F. Wang and F. Shao, *Nature*, 2015, **526**, 660–665.
13 T. Bergsbaken, S. L. Fink and B. T. Cookson, *Nat. Rev. Microbiol.*, 2009, **7**, 99–109.
14 H. Im and A. Ammit, *Clin. Exp. Allergy*, 2014, **44**, 160–172.
15 S. L. Fink and B. T. Cookson, *Cell. Microbiol.*, 2006, **8**, 1812–1825.
16 I. Zanoni, Y. Tan, M. Di Gioia, A. Broggi, J. Ruan, J. Shi, C. A. Donado, F. Shao, H. Wu and J. R. Springstead, *Science*, 2016, **352**, 1232–1236.
17 V. I. Maltez, A. L. Tubbs, K. D. Cook, Y. Aachoui, E. L. Falcone, S. M. Holland, J. K. Whitmire and E. A. Miao, *Immunity*, 2015, **43**, 987–997.
18 C. L. Evavold, J. Ruan, Y. Tan, S. Xia, H. Wu and J. C. Kagan, *Immunity*, 2018, **48**, 35–44.
19 M. Rossi and J. W. Young, *J. Immunol. Res.*, 2005, **175**(3), 1373–1381.
20 W. Zou, *Nat. Rev. Cancer*, 2005, **5**, 263–274.
21 P. Gotwals, S. Cameron, D. Cipolletta, V. Cremasco, A. Crystal, B. Hewes, B. Mueller, S. Quaratino, C. Sabatos-Peyton and L. Petruzzelli, *Nat. Rev. Cancer*, 2017, **17**, 286–301.
22 J. Banchereau and A. K. Palucka, *Nat. Rev. Immunol.*, 2005, **5**, 296–306.
23 S. Wang, Z. Sun and Y. Hou, *Adv. Healthc. Mater.*, 2020, 2000845.
24 E. Yuba, A. Yamaguchi, Y. Yoshizaki, A. Harada and K. Kono, *Biomaterials*, 2017, **120**, 32–45.
25 E.-J. Ko, Y.-T. Lee, Y. Lee, K.-H. Kim and S.-M. Kang, *Immune Netw.*, 2017, **17**, 326–342.
26 G. L. Beatty, E. G. Chiorean, M. P. Fishman, B. Saboury, U. R. Teitelbaum, W. Sun, R. D. Huhn, W. Song, D. Li and L. L. Sharp, *Science*, 2011, **331**, 1612–1616.
27 A. Amedei, D. Prisco and M. M. D'Elios, *Recent Pat. Anti-Canc.*, 2013, **8**, 126–142.
28 H. Wang and D. J. Mooney, *Nat. Mater.*, 2018, **17**, 761–772.
29 C. M. Le Gall, J. Weiden, L. J. Eggermont and C. G. Figdor, *Nat. Mater.*, 2018, **17**, 474–475.
30 C. R. Perez and M. De Palma, *Nat. Commun.*, 2019, **10**, 1–10.
31 Z. Y. Wu, H. J. Wang, L. L. Ma, J. Xue and J. H. Zhu, *Microporous Mesoporous Mater.*, 2008, **109**, 436–444.
32 L. M. Kustov and V. B. Kazansky, *J. Chem. Soc., Faraday Trans.*, 1991, **87**, 2675–2678.
33 L. D. Rollmann, in *Zeolites: Science and Technology*, Springer, 1984, pp. 109–126.
34 V. Verdoliva, M. Saviano and S. De Luca, *Catalysts*, 2019, **9**, 248.
35 Y. Yang, J. Tang, H. Song, Y. Yang, Z. Gu, J. Fu, Y. Liu, M. Zhang, Z. A. Qiao and C. Yu, *Angew. Chem., Int. Ed.*, 2020, **132**(44), 19778–19785.
36 M. A. Katsnelson, L. G. Rucker, H. M. Russo and G. R. Dubyak, *J. Immunol.*, 2015, **194**, 3937–3952.
37 Y. Yang, S. Bernardi, H. Song, J. Zhang, M. Yu, J. C. Reid, E. Strounina, D. J. Searles and C. Yu, *Chem. Mater.*, 2016, **28**, 704–707.
38 D. Shen, J. Yang, X. Li, L. Zhou, R. Zhang, W. Li, L. Chen, R. Wang, F. Zhang and D. Zhao, *Nano Lett.*, 2014, **14**, 923–932.
39 E. Shardlow, M. Mold and C. J. F. i. c. Exley, *Front. Chem.*, 2017, **4**, 48.
40 X. Li, S. Hufnagel, H. Y. Xu, S. A. Valdes, S. G. Thakkar, Z. R. Cui and H. Celio, *ACS Appl. Mater. Interfaces*, 2017, **9**, 22893–22901.
41 W. Rongchapo, C. Keawkumay, N. Osakoo, K. Deekamwong, N. Chanlek, S. Prayoonpokarach and J. Wittayakun, *Adsorpt. Sci. Technol.*, 2018, **36**, 684–693.
42 M. J. Stephenson, S. M. Holmes and R. A. Dryfe, *Angew. Chem., Int. Ed.*, 2005, **44**, 3075–3078.
43 K. H. Lim and C. P. Grey, *J. Am. Chem. Soc.*, 2000, **122**, 9768–9780.
44 Y. Ono, *J. Catal.*, 2003, **216**, 406–415.
45 C. Martineau, F. Taulelle and M. Haouas, *PATAI'S Chemistry of Functional Groups*, 2009, pp. 1–51.
46 G. Panyi, Z. Varga and R. Gáspár, *Immunol. Lett.*, 2004, **92**, 55–66.
47 K. Kis-Toth, P. Hajdu, I. Bacskai, O. Szilagyi, F. Papp, A. Szanto, E. Posta, P. Gogolak, G. Panyi and E. Rajnavolgyi, *J. Immunol.*, 2011, **187**, 1273–1280.
48 E. Zsiros, K. Kis-Toth, P. Hajdu, R. Gaspar, J. Bielanska, A. Felipe, E. Rajnavolgyi and G. Panyi, *J. Immunol.*, 2009, **183**, 4483–4492.
49 Y. Pirahanchi and N. R. Aeddula, in *StatPearls*, StatPearls Publishing, 2019.
50 R. Muñoz-Planillo, P. Kuffa, G. Martínez-Colón, B. L. Smith, T. M. Rajendiran and G. Núñez, *Immunity*, 2013, **38**, 1142–1153.
51 A. Di, S. Xiong, Z. Ye, R. S. Malireddi, S. Kometani, M. Zhong, M. Mittal, Z. Hong, T.-D. Kanneganti and J. Rehman, *Immunity*, 2018, **49**, 56–65.
52 D. J. Aidley and P. R. Stanfield, *Ion channels: molecules in action*, Cambridge University Press, 1996.
53 H. Hentze, X. Y. Lin, M. S. K. Choi and A. G. Porter, *Cell Death Differ.*, 2003, **10**, 956–968.
54 B. O'Rourke, *Annu. Rev. Physiol.*, 2007, **69**, 19–49.
55 S. Cermak, M. Kosicek, A. Mladenovic-Djordjevic, K. Smiljanic, S. Kanazir and S. Hecimovic, *PLoS One*, 2016, **11**, e0167428.
56 M. Moossavi, N. Parsamanesh, A. Bahrami, S. L. Atkin and A. Sahebkar, *Mol. Cancer*, 2018, **17**, 158.
57 E. Latz, T. S. Xiao and A. Stutz, *Nat. Rev. Immunol.*, 2013, **13**, 397–411.
58 M. T. Orr, A. P. Khandhar, E. Seydoux, H. Liang, E. Gage, T. Mikasa, E. L. Beebe, N. D. Rintala, K. H. Persson and A. Ahniyaz, *npj Vaccines*, 2019, **4**, 1–10.
59 W.-t. He, H. Wan, L. Hu, P. Chen, X. Wang, Z. Huang, Z.-H. Yang, C.-Q. Zhong and J. Han, *Cell Res.*, 2015, **25**, 1285–1298.
60 X. Chen, W.-t. He, L. Hu, J. Li, Y. Fang, X. Wang, X. Xu, Z. Wang, K. Huang and J. Han, *Cell Res.*, 2016, **26**, 1007–1020.
61 J. S. Tsau, X. Huang, C.-Y. Lai and S. M. Hedrick, *J. Immunol.*, 2018, **200**, 1335–1346.

62 H. Liu, K. D. Moynihan, Y. Zheng, G. L. Szeto, A. V. Li, B. Huang, D. S. Van Egeren, C. Park and D. J. Irvine, *Nature*, 2014, **507**, 519–522.
63 H. Ruan, B. J. Leibowitz, L. Zhang and J. Yu, *Mol. Carcinog.*, 2020, **59**, 783–793.
64 U. Kalina, D. Kauschat, N. Koyama, H. Nuernberger, K. Ballas, S. Koschmieder, G. Bug, W.-K. Hofmann, D. Hoelzer and O. G. Ottmann, *J. Immunol.*, 2000, **165**, 1307–1313.
65 E. Lion, E. L. J. M. Smits, Z. N. Berneman and V. F. I. Van Tendeloo, *J. Immunol. Methods*, 2009, **350**, 89–96.
66 C. Ménard, J.-Y. Blay, C. Borg, S. Michiels, F. Ghiringhelli, C. Robert, C. Nonn, N. Chaput, J. Taïeb, N. F. Delahaye, C. Flament, J.-F. Emile, A. Le Cesne and L. Zitvogel, *Cancer Res.*, 2009, **69**, 3563–3569.
67 T. Strowig, F. Brilot and C. Münz, *J. Immunol.*, 2008, **180**, 7785–7791.
68 Y. Huang, H. Wang, Y. Hao, H. Lin, M. Dong, J. Ye, L. Song, Y. Wang, Q. Li and B. Shan, *Nat. Cell Biol.*, 2020, 1–12.
69 Y.-Q. Wang, H. Bazin-Lee, J. T. Evans, C. R. Casella and T. C. Mitchell, *Front. Immunol.*, 2020, **11**, 2716.
70 M. K. MacLeod, A. S. McKee, A. David, J. Wang, R. Mason, J. W. Kappler and P. Marrack, *Proc. Natl. Acad. Sci. U.S.A.*, 2011, **108**, 7914–7919.
71 M.-A. Lacaille-Dubois, *Phytomedicine*, 2019, **60**, 152905.